GAEP1226-0102
Jan. 23, 2026
by K. Tomisaka

3: Low Metallicity Gas on the Outskirts of the Local Group: the Circumgalactic Medium of Sextans B
Authors: Andrew J. Fox+, ApJ accepted

31: A millimeter methanol maser ring tracing the deceleration of the heat wave powered by the massive protoste
Authors: T. R. Hunter+, ApJL accepted

44: SiO emission in the filamentary Infrared Dark Cloud G035.39-00.33: An ALMA view
Authors: Rong Liu+ accepted for AAp

69: A large, long-lived, slowly-expanding superbubble across the Perseus Arm
Authors: Bingqiu Chen+Nature Communications, 16, 10558(2025)

32: From Nbody1 to Nbody7: the Growth of Sverre's Industry
Authors: Rainer Spurzem

60: Chain Reactions in Space: Analyzing the Impact of Satellite Collisions and Debris Accumulation
Authors: Mark Ballard, Guanqun Song, Ting Zhu

3: 2601.00437

Low Metallicity Gas on the Outskirts of the Local Group: the Circumgalactic Medium of Sextans B

Authors: Andrew J. Fox+, ApJ accepted

Abstract: We present a UV absorption-line analysis of the circumgalactic medium (CGM) of Sextans B, a dwarf irregular galaxy at 1.3 Mpc distance on the outer frontier of the Local Group. Using HST/COS spectroscopy of two AGN sightlines passing through the Sextans B CGM at small impact parameters of 4 kpc and 8 kpc (0.04 and 0.08 r_vir), we detect the CGM in Si II, Si III, Si IV, and C II absorption. All four ions show a column-density profile that declines with radius. The profiles fall below the average CGM profiles of other nearby dwarfs (by 0.3-0.6 dex, depending on ion), likely due to the low halo mass and low metallicity of Sextans B. Using Cloudy photoionization models and interferometric measurements of the H I column density, we find low gas-phase silicon and carbon abundances in the Sextans B CGM, [Si/H]=-1.7+/-0.2 and [C/H]=-2.1+/-0.2, among the lowest gas-phase abundances anywhere in the Local Group. We calculate a cool CGM gas mass within 8 kpc of , comparable to the H I mass and the stellar mass of Sextans B.

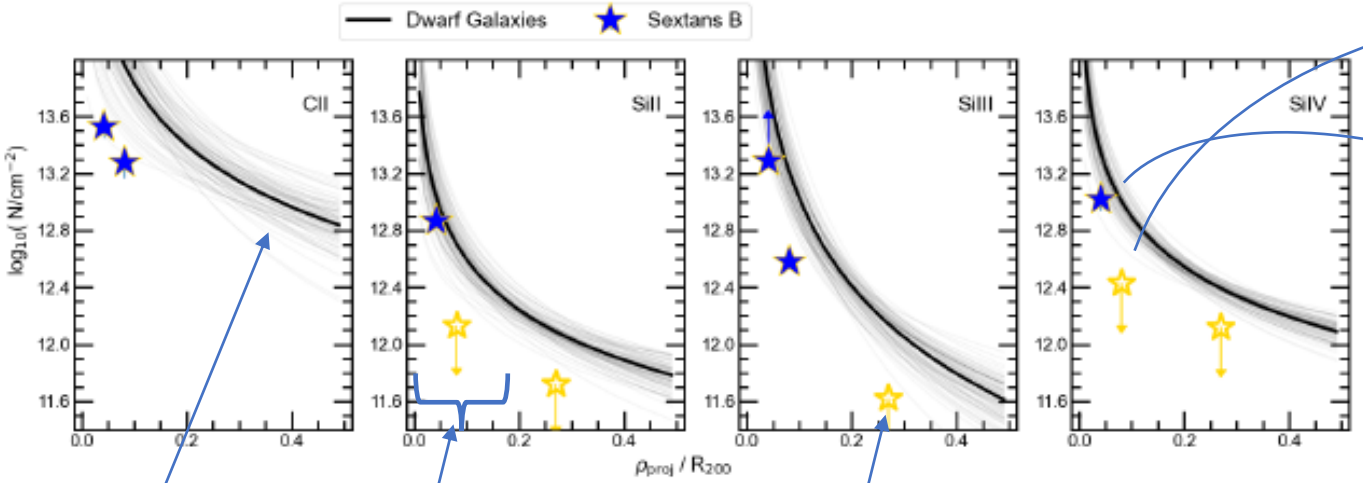

論文の点

Zheng+ 2024

Local Group dwarf G.

similar to stellar metallicity [Fe/H]=-1.9

radiation ionization equilibrium by Cloudy

prediction

Obs

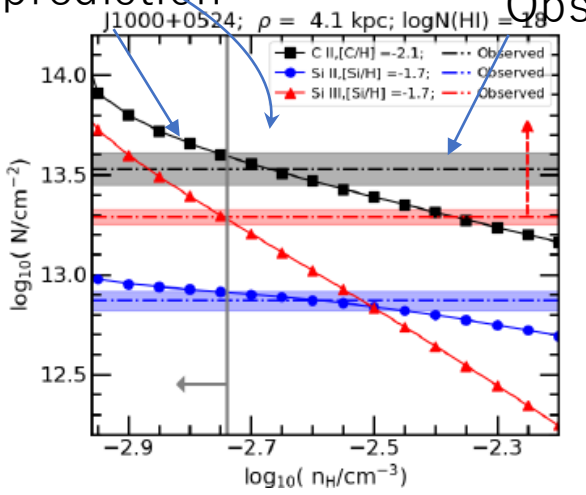

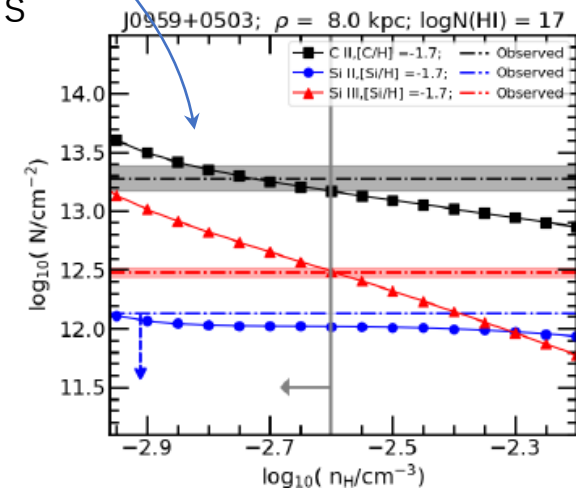

dust depletion??
nucleosynthesis
∧
[C/H]=-2.1,
[Si/H]=-1.7

local density
[C/H]=-1.7,
[Si/H]=-1.7

31: 2512.24380

A millimeter methanol maser ring tracing the deceleration of the heat wave powered by the massive protostellar accretion outburst in G358.93-0.03 MM1
Authors: T. R. Hunter+, ApJL accepted

Abstract: We present multi-epoch, multi-band ALMA imaging of the new Class II millimeter methanol masers excited during the accretion outburst of the massive protostar G358.93-0.03 MM1. The highest angular resolution image (24 mas 160 au) reveals a nearly complete, circular ring of strong maser spots in the 217.2992 GHz (=1) maser line that closely circumscribes the dust continuum emission from MM1. Weaker maser emission lies inside the eastern and southern halves of the maser ring, generally coincident with the centimeter masers excited during the outburst, but avoiding the densest parts of the hot core gas traced by high excitation lines of CHCN. Using a variety of fitting techniques on the image cubes of the two strongest maser lines, each observed over 3-4 epochs, we find the diameter of the ring increased by 60% (from 1100 to 1800 au in the 217 GHz line) over 200 days, consistent with an average radial propagation rate of 0.01c, while the maser intensity declined exponentially. Fitting the angular extent of the millimeter masers versus time yields a power law of index 0.390.06, which also reproduces the observed extent of the 6.7 GHz masers in the first VLBI epoch of R. A. Burns et al. (2020). This exponent is consistent with the prediction of radius vs. time in the Taylor-von Neumann-Sedov self-similar solution for an intense spherical explosion from a point source (R ∝ t^2/5). These results demonstrate the explosive nature of accretion outbursts in massive protostars and their ability to generate subluminal heat waves traceable by centimeter and millimeter masers for several months as the energy traverses the surrounding molecular material.

Class II methanol maser: pumped by IR photons

@Jan.14,2019, first outburst is observed
compact clump (1.1mmBolocam; 0.87mm Atlas Gal)
D=6.7kpc

Main properties of outbursting HMYSOs.

V. G. Elbakyan+2024

Object	Mass [$M_\odot$]	Radius [$R_\odot$]	Burst duration [yr]	Rise time [yr]	$\dot{M}_{peak}$ [$M_\odot$ yr^{-1}]	Accreted mass [M_J]	Multiple bursts
M17 MIR (§)	5.4	10.1 – 34.1	9 – 20	< 1	5×10^{-3}, 2×10^{-3}	~30(×2)	Yes
NGC 6334I MM1 (*)	6.7	2.6 – 20	> 8	$0.62^{+0.14}_{-0.14}$	2.3×10^{-3}	$0.325^{+0.126}_{-0.094}$	No
G358.93–0.03 MM1 (‡)	$9.7^{+0.3}_{-0.6}$	$3.9^{+0.1}_{-0.2}$	0.75	$0.16^{+0.01}_{-0.01}$	$1.8^{+1.2}_{-1.1} \times 10^{-3}$	0.566	No
V723 Car (¶)	10	18 – 58	5	4	–	–	No?
S255IR NIRS 3 (†)	20	10	2 – 2.5	0.4	5×10^{-3}	2	Yes ($)
G323.46–0.08 (**)	23	–	8.4	1.4	0.8×10^{-3}		
W51 IRS2 (·)	40–60 (▽)	–	< 1	≪1	–	~260(0.25 $M_\odot$)	No

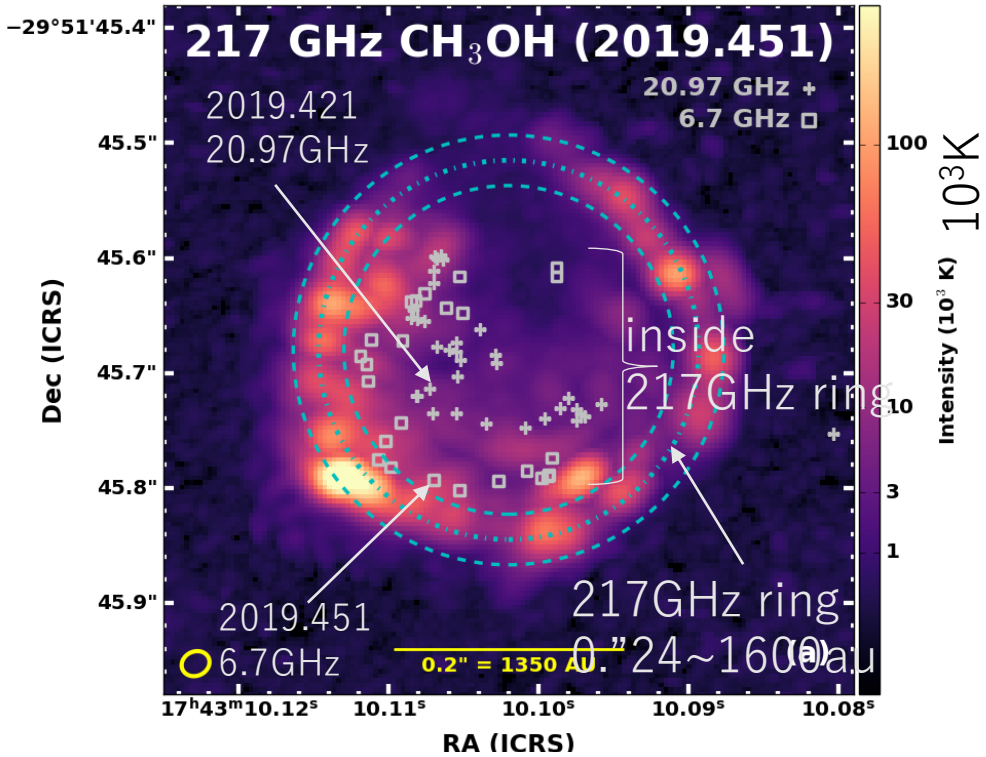
217 GHz CH3OH (2019.451)
20.97 GHz +
6.7 GHz
2019.421
20.97GHz
inside
217GHz ring
2019.451
6.7GHz
217GHz ring-
0."24~1600au
0.2" = 1350 AU.
Dec (ICRS)
RA (ICRS)
Intensity (10³ K)
10³K

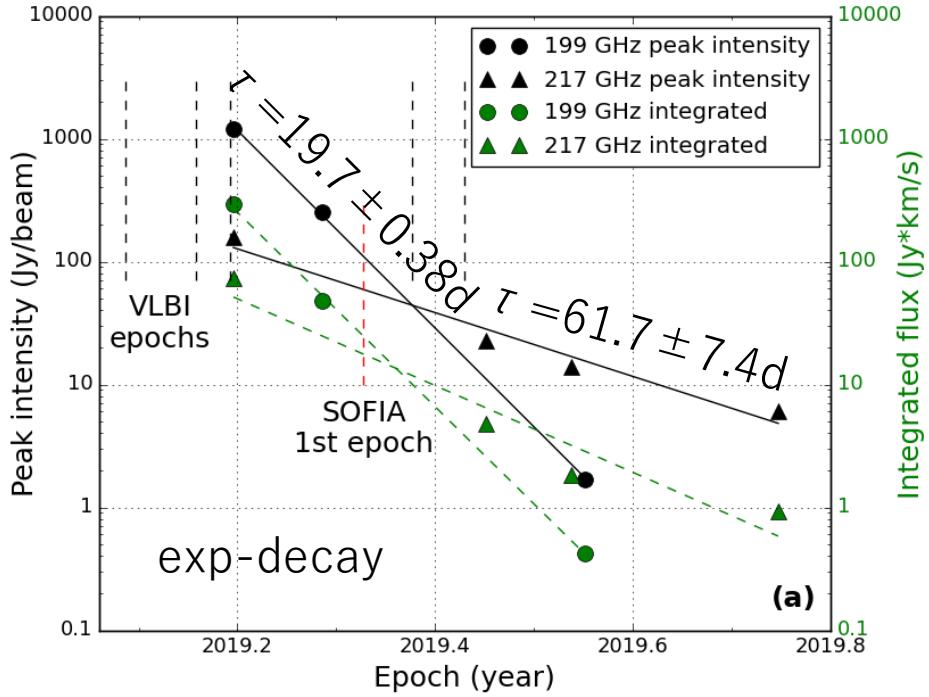
199 GHz peak intensity
217 GHz peak intensity
199 GHz integrated
217 GHz integrated
τ =19.7±0.38d
τ =61.7±7.4d
VLBI
epochs
SOFIA
1st epoch
exp-decay
(a)
Peak intensity (Jy/beam)
Integrated flux (Jy*km/s)
Epoch (year)

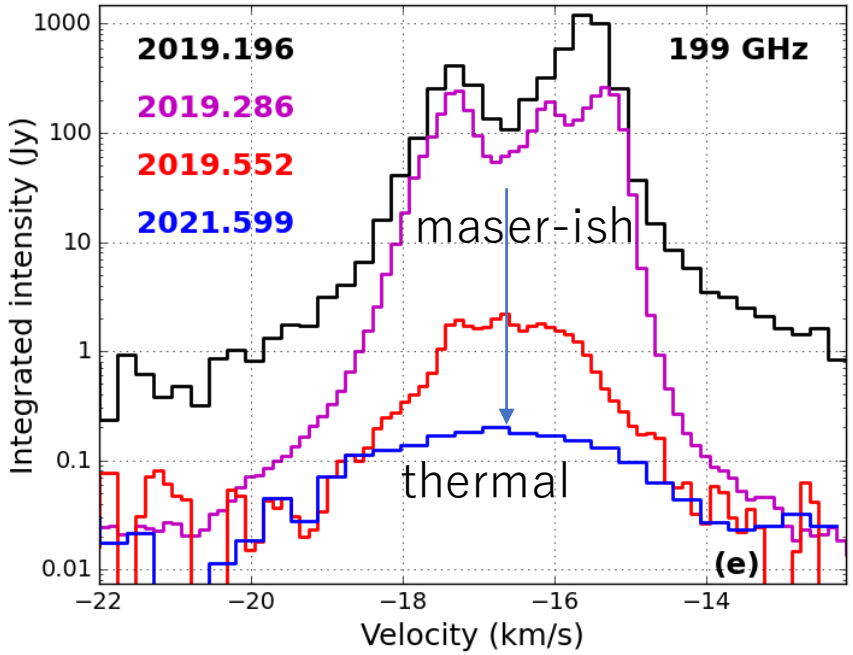
2019.196
2019.286
2019.552
2021.599
199 GHz
maser-ish
thermal
(e)
Integrated intensity (Jy)
Velocity (km/s)

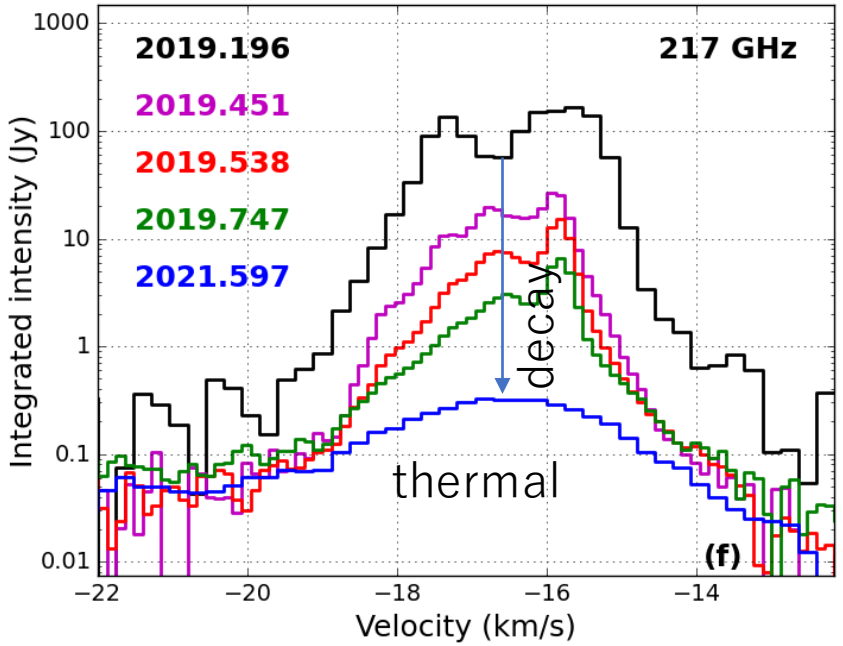
2019.196
2019.451
2019.538
2019.747
2021.597
217 GHz
decay
thermal
(f)
Integrated intensity (Jy)
Velocity (km/s)

two-component fitting

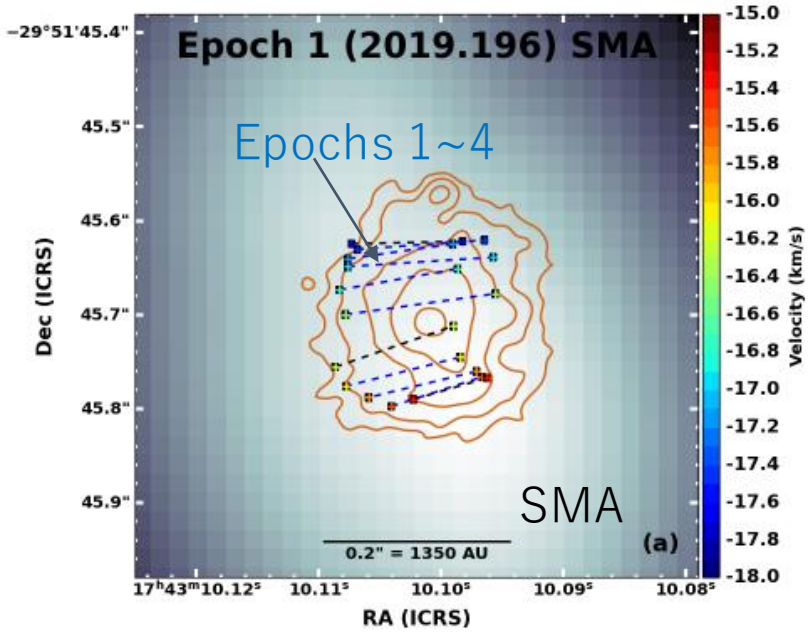

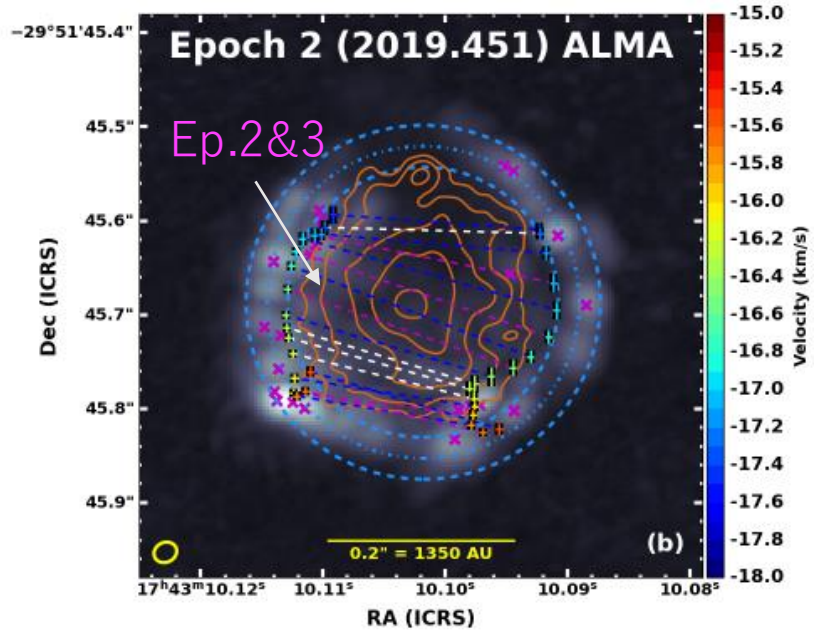

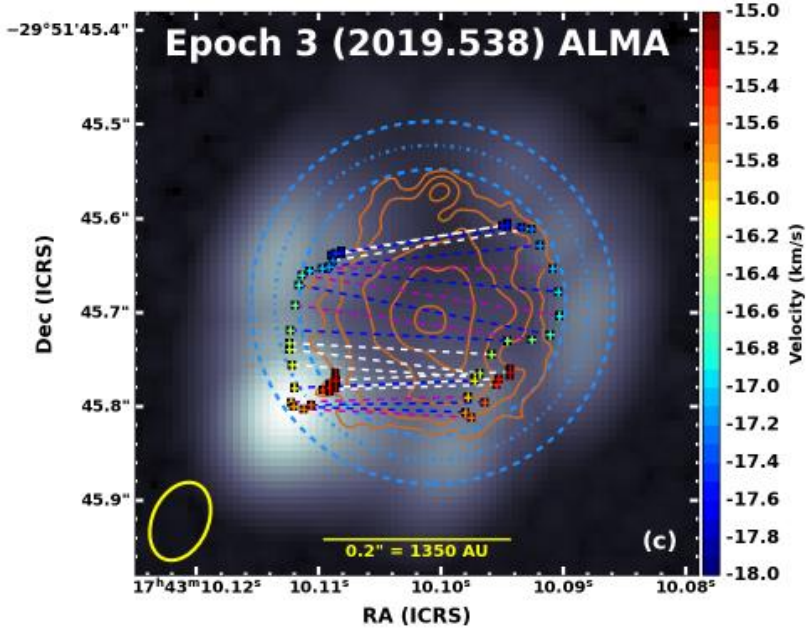

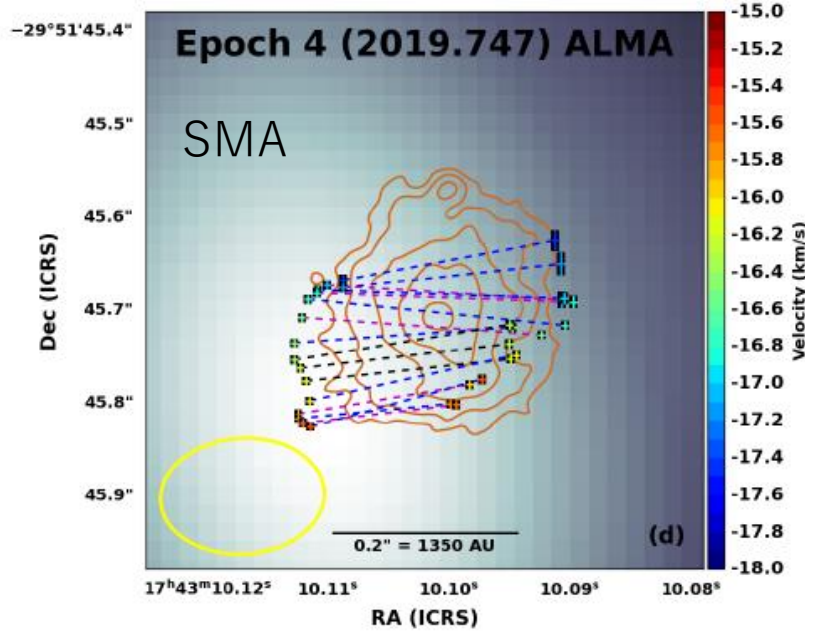

deconvolve into pair maser spots with different velocities

blue: consistent through 4 epochs
magenta: consistent for alma epochs
white/black: others

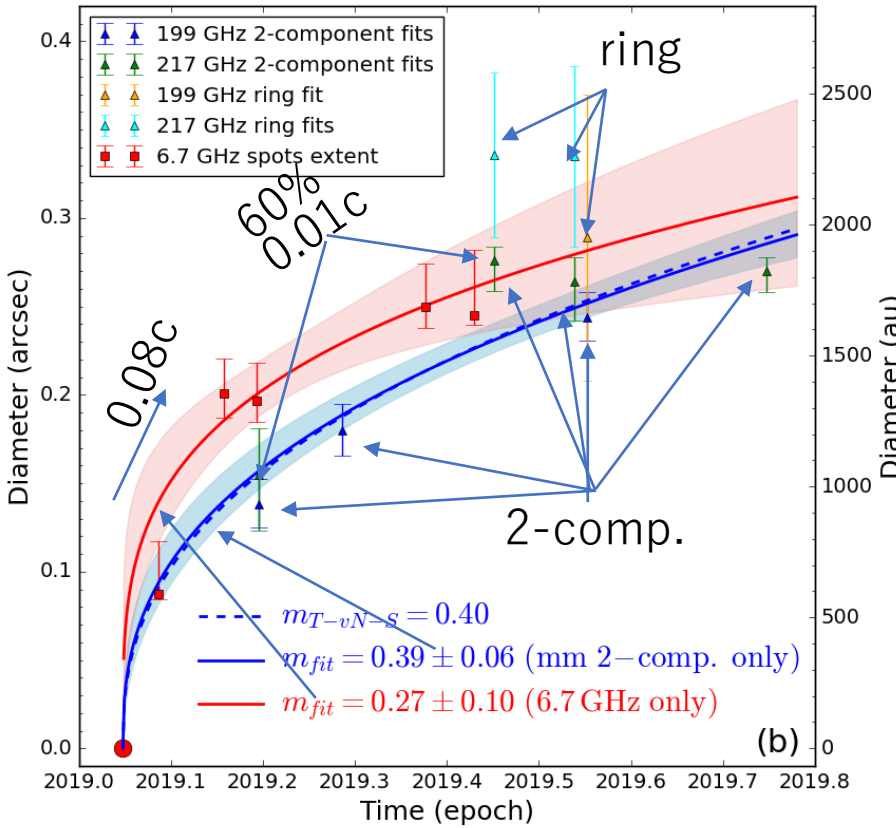

Abstract: Filamentary infrared dark clouds (IRDCs) are believed to represent the initial conditions for massive star and cluster formation. We investigate the IRDC G035.39-00.33 using SiO, H13CO+, CH3OH, and CS emission observed with ALMA at 3.5\arcsec\ resolution (0.05 pc). The SiO emission traces shock activity within the cloud, providing insights into current star formation and cloud formation mechanisms. We identify several regions with broad SiO emission clearly associated with outflows, pinpointing the locations of ongoing star formation across the cloud. The ALMA images also reveal a series of spatially extended SiO emission spots with narrow line profiles, aligned along an arc-like path that is also seen in CS and CH3OH emission. While the broad SiO emission is mainly associated with the main cloud filament, as seen in visual extinction, the narrow SiO arch is located at the edge of the cloud, far from the identified sites of star formation activity. The presence of these arc-like morphologies suggests that large-scale shocks may have compressed the gas in the surroundings of the G035.39-00.33 cloud, shaping its filamentary structure. By inspecting the large-scale radio continuum emission around G035.39-00.33, we find that this IRDC is part of a larger star-forming complex where the densest and coolest material appears at the interacting regions between a Supernova Remnant (SNR) and an expanding HII region. In particular, we hypothesize that this IRDC may be spatially coincident with the ionized expanding gas associated with the previously identified SNR G35.6-0.4. We suggest that collisions between giant molecular clouds and expanding gas flows from interacting SNRs and HII regions may be responsible for the observed arc-like structures. Such shock compressions could play an important role in the formation of IRDCs and in the potential triggering of star formation.

44: 2512.23384

SiO emission in the filamentary Infrared Dark Cloud G035.39-00.33: An ALMA view

Authors: Rong Liu+

accepted for AAp

3-color image

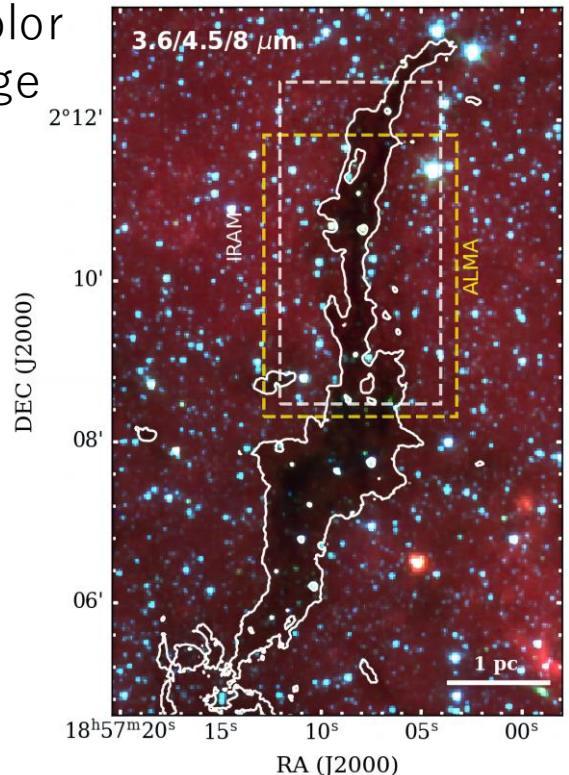

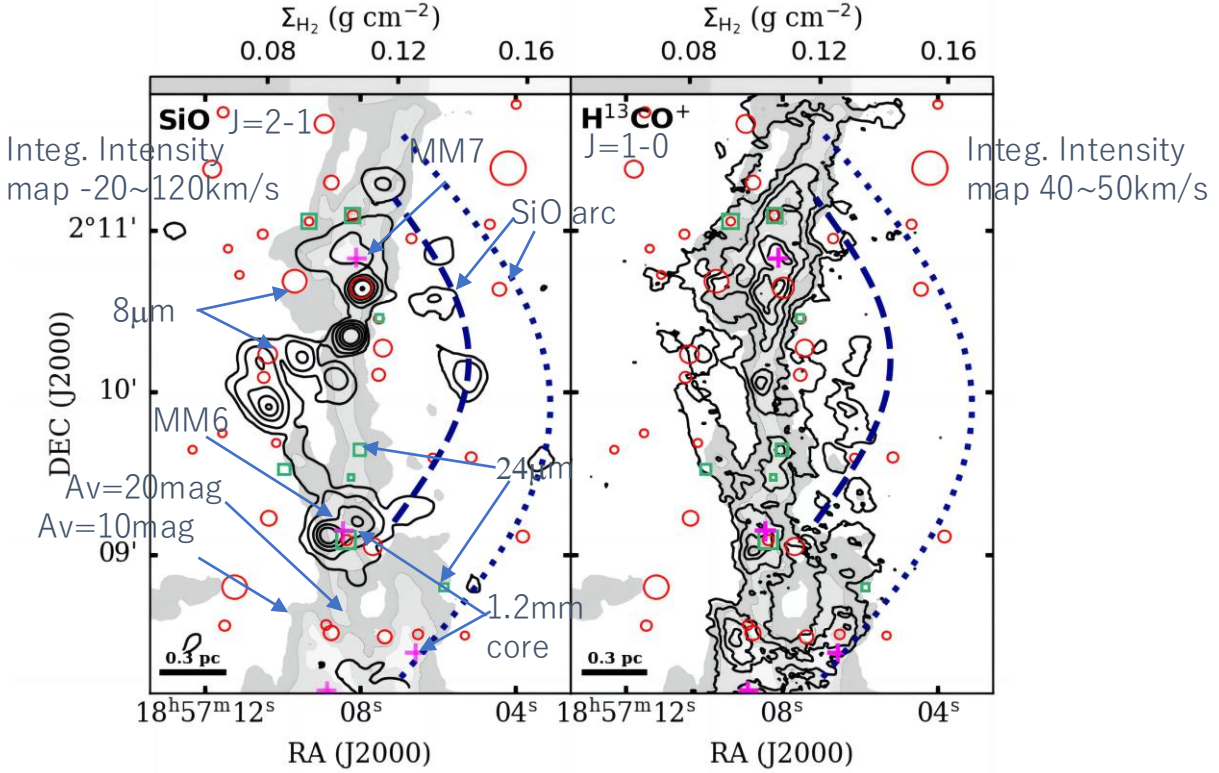

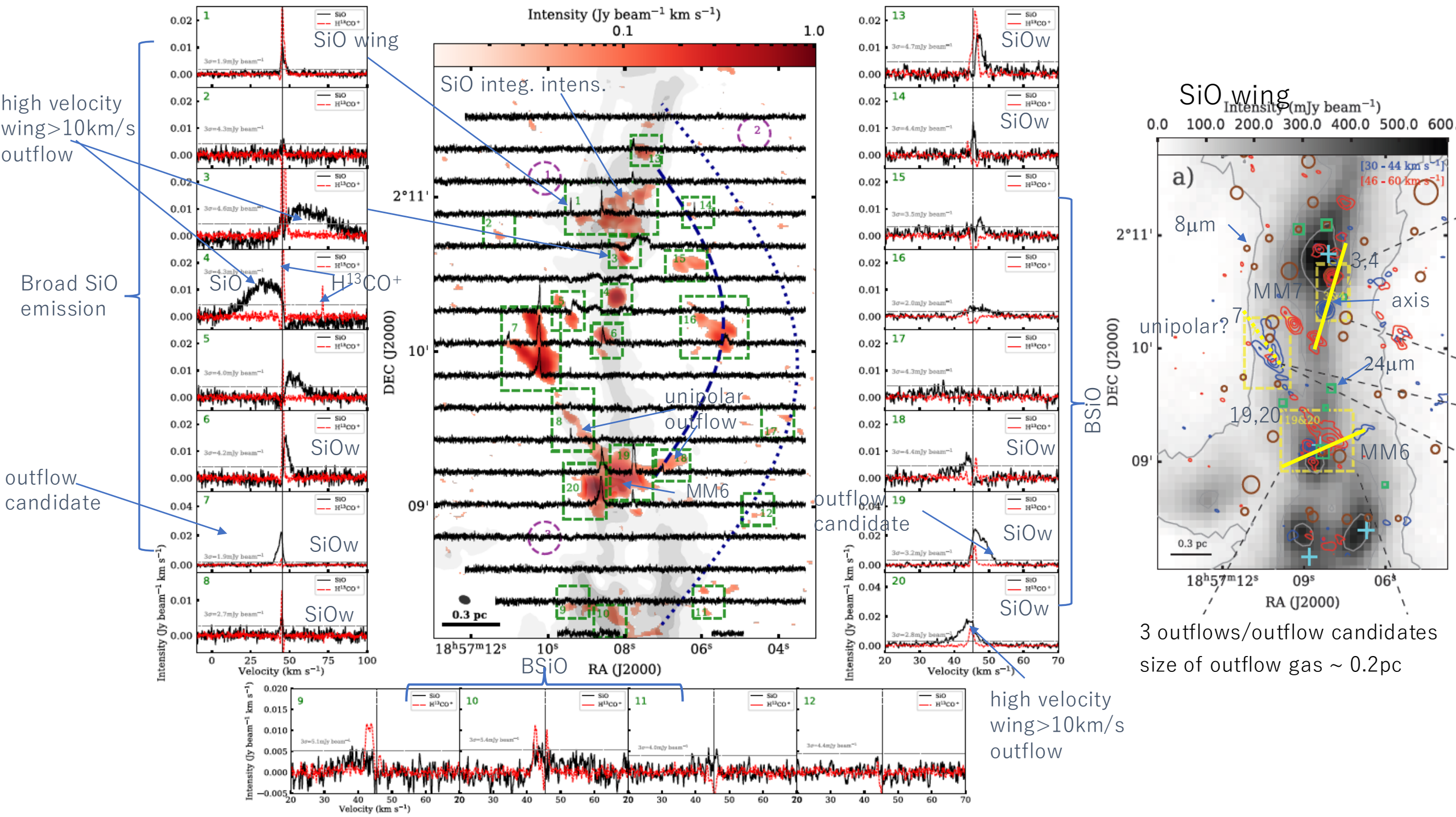
high velocity wing>10km/s outflow
Broad SiO emission
outflow candidate
SiO wing
SiO integ. intens.
SiO
H13CO+
SiOw
unipolar outflow
MM6
BSiO
outflow candidate
high velocity wing>10km/s outflow
Intensity (Jy beam−1 km s−1)
Velocity (km s−1)
DEC (J2000)
RA (J2000)
0.3 pc
SiO wing
Intensity (mJy beam−1)
[30 - 44 km s−1]
[46 - 60 km s−1]
a)
8μm
24μm
3,4
MM7
axis
unipolar?
7
19,20
MM6
3 outflows/outflow candidates
size of outflow gas ~ 0.2pc

Outflow quantities from SiO

point	core	$M_{out}(M_\odot)$	$MV(M_\odot km/s)$	E(erg)	$T_{dyn}(yr)$	$dM/dt(M_\odot yr^{-1})$	$MV/t_{dyn}(M_\odot km\ s^{-1}yr^{-1})$	$L(L_\odot)$
3,4	MM7	1.8	27.5	4.2×10^{45}	9.3×10^{3}	2×10^{-4}	3×10^{-3}	3.7
7	Rb-sym.	2.1	5.1	1.2×10^{44}	5.4×10^{4}	3.9×10^{-5}	9.4×10^{-5}	0.02
19,20	MM6	1.4	5.0	1.9×10^{44}	2.5×10^{4}	5.4×10^{-5}	2×10^{-4}	0.06

Typical for high mass protostars

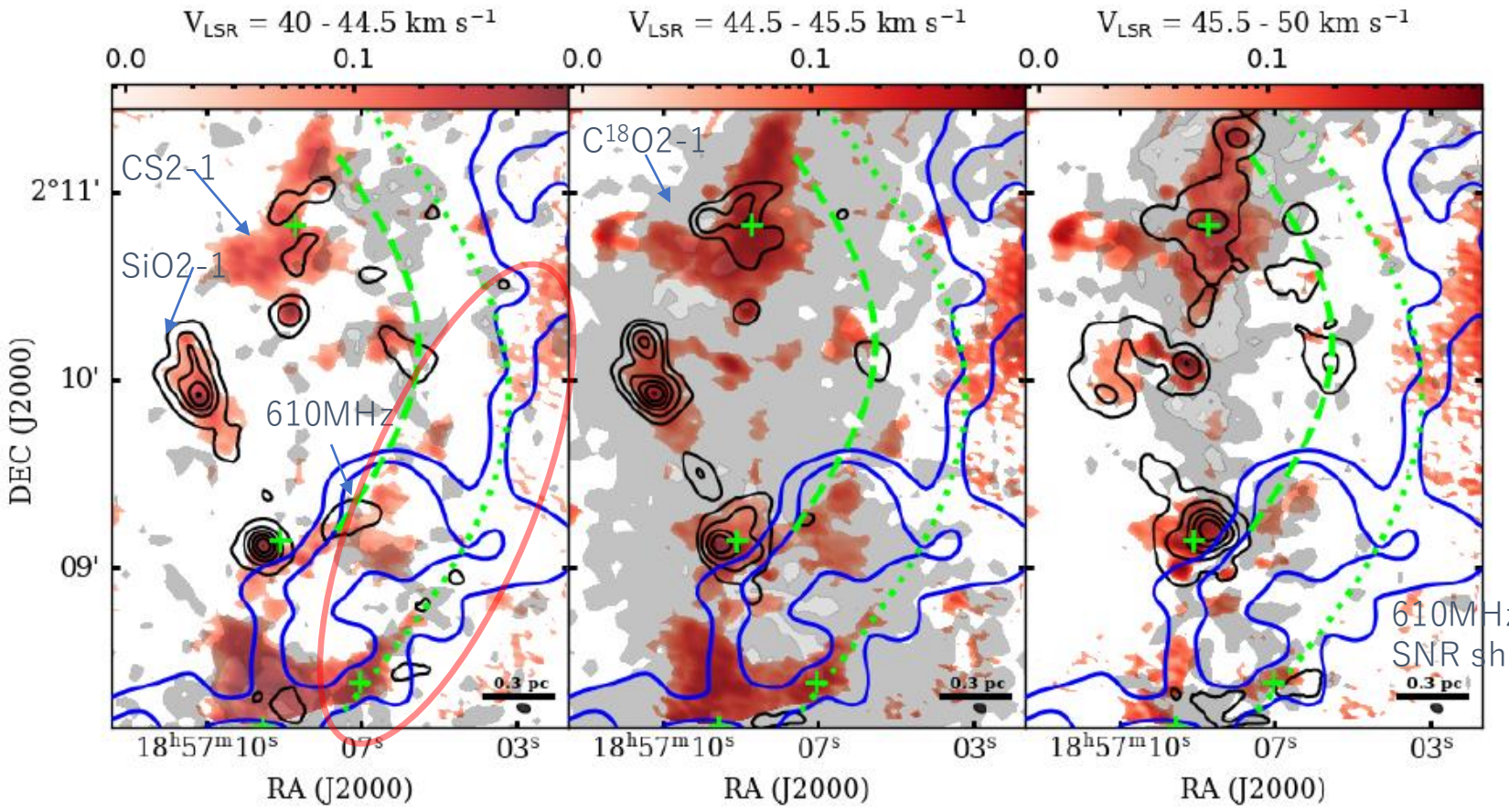

CS brightest: middle velocity range
CS <44.5km/s >45.5km/s
two arc-like structures??
$C^{18}O$ 2-1 also follows inner arc.

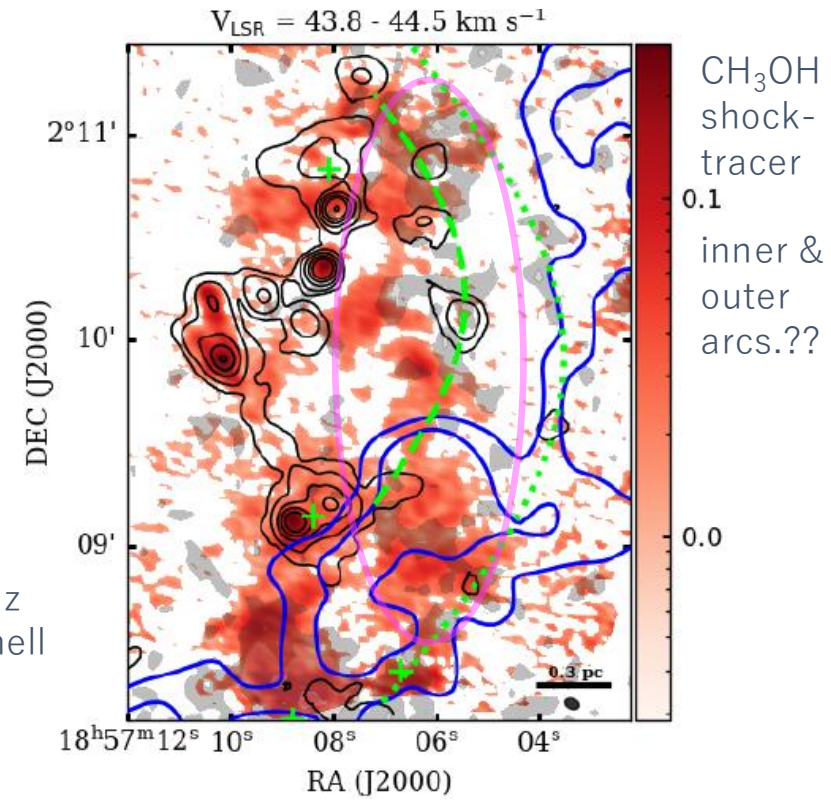

SNR-filament link
W44 -- IRDC G034.77-00.55 (Cosentino+ 2019)
SNR G35.6-0.6 – Cloud H

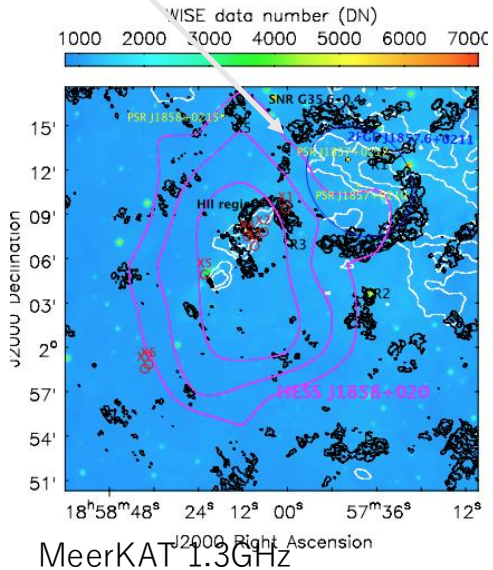

GMRT 610MHz
Paredes+2014

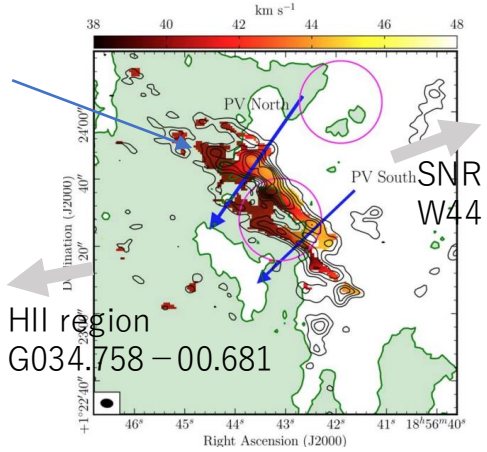

MeerKAT 1.3GHz
Goedhald+2024

GLOSTAR 5.6GHz
Medina+2019

FUGIN ^{13}CO1-0
Umemoto+2017

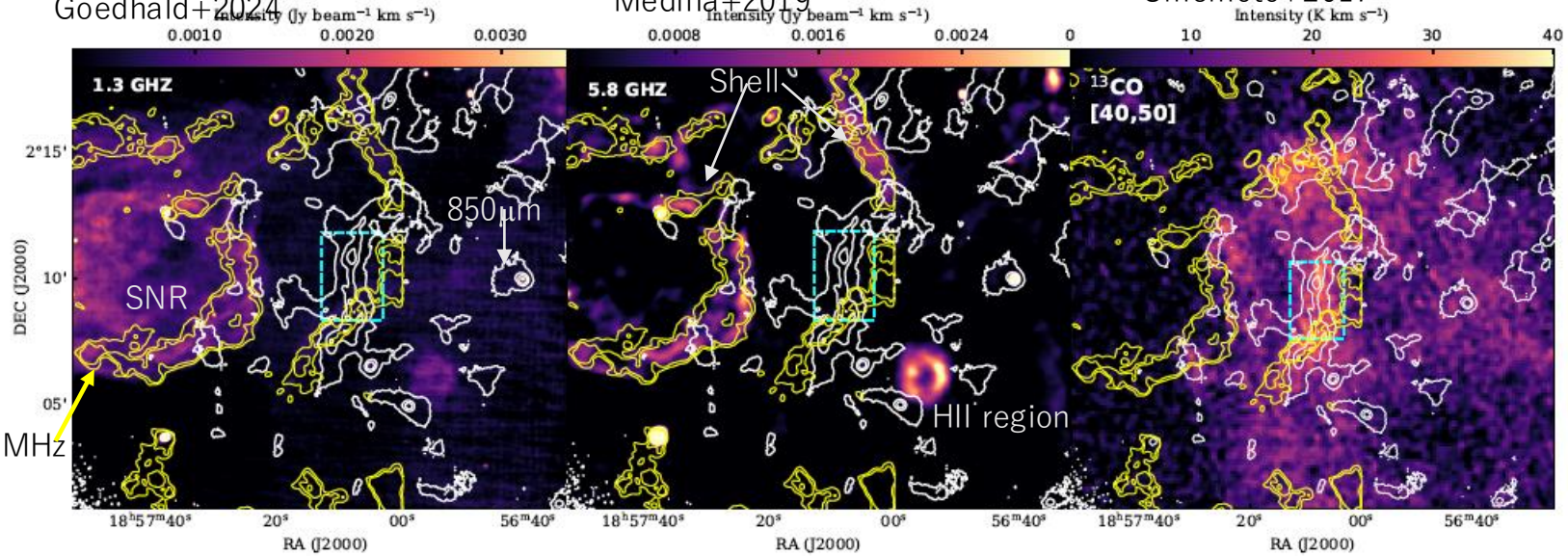

★610MHz: SNR 2nd shell
// IRDC filament
same curvature of SiO (CS, C18O,..) arc

★These observations indicate that Cloud H is embedded within a complex star-forming environment, where the densest and coolest material appears to be concentrated at the interface between SNR G35.6-0.4 and the expanding Hii region.

69: 2512.21927

A large, long-lived, slowly-expanding superbubble across the Perseus Arm

Authors: Bingqiu Chen+Nature Communications, 16, 10558(2025)

Abstract: Stellar feedback is a crucial mechanism in galactic evolution, as demonstrated by the widespread bubbles observed with JWST. In this study, we combine data from Gaia and LAMOST to obtain a sample of young O-B2 stars with full three-dimensional velocity information. Focusing on the largest known superbubble in the Milky Way, we identify groups of O-B2 stars at its periphery, exhibiting a transverse velocity of 25.8 km/s and an expansion velocity of 6.2 km/s. Using these velocities, we calculate a crossing time t_cross ~ 20 Myr and an expansion timescale t_expansion ~ 80 Myr. We estimate a survival timescale t_survival ~ 250 Myr and a supernova interval t_SN ~ 0.1 Myr. Together with the Galactic shear timescale t_shear ~ 30 Myr, these values satisfy t_SN < t_shear < t_survival. The energy and momentum from supernovae are sufficient to sustain the bubble's growth against ambient pressure. This indicates that repeated supernovae replenish energy faster than shear and turbulent distort the cavity. Our analysis classifies the Giant Oval Cavity as a large, quasi-stationary superbubble, similar to the Phantom Bubble observed by JWST, stabilised by the interplay between stellar feedback and Galactic disk dynamics.

O-B2 stars(τ<20Myr, LAMOST+Gaia)

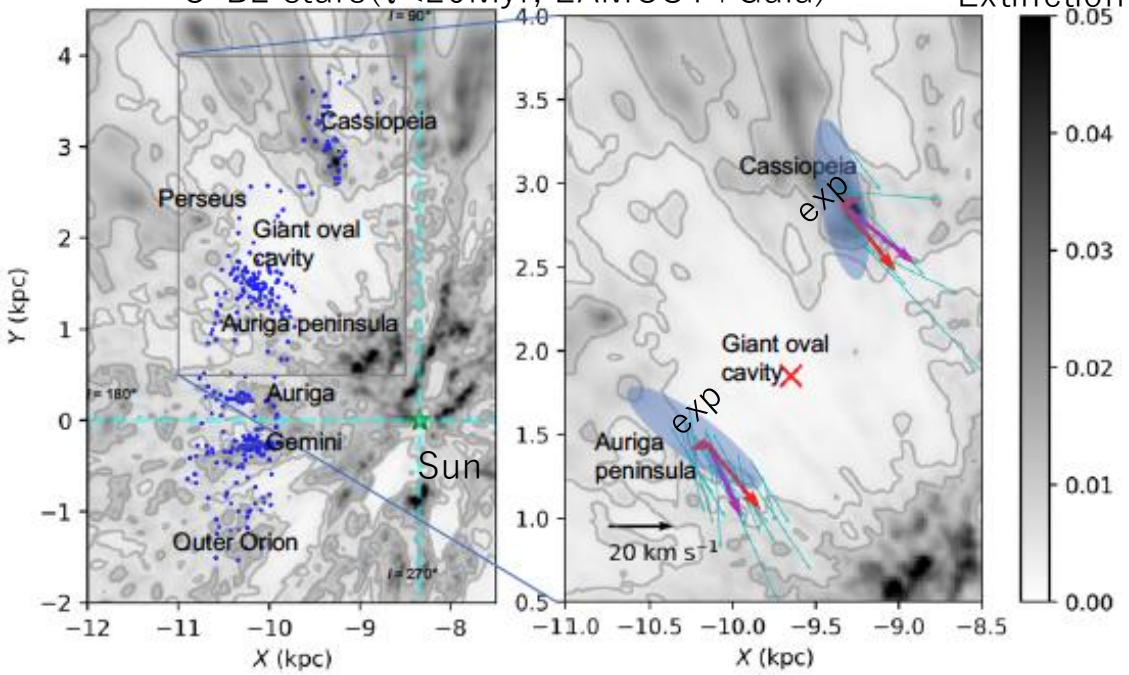

Extinction

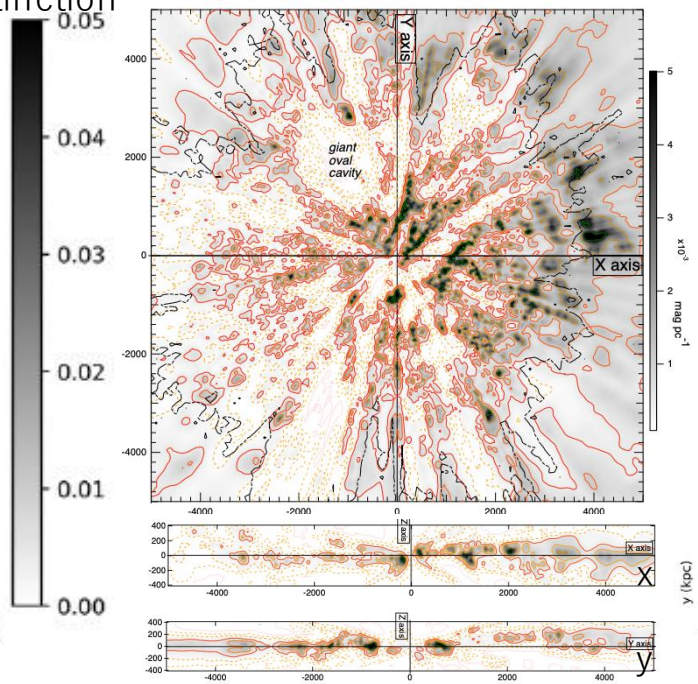

Vergely+20

expansion $6.2 \pm 2 kms^{-1}$ D~1kpc
cf local buble $5.5 kms^{-1}$ D~200pc
shared peculiar velocity $25.6 \pm 3 kms^{-1}$
$t_{exp} \sim (D/2)/v_{exp} \sim 500pc/6.2 kms^{-1} \sim 80Myr$
$t_{sur} \sim D/\sigma_{turb} \sim 1kpc/4 kms^{-1} \sim 250Myr$
$t_{SN} \sim 1/n_{SN}D^2 \sim 1/0.01 pc^{-2}Gyr^{-1}/10^6 pc^2$
~0.1Myr
$t_{shear} \sim 30Myr$

large+stationary vs small+transient

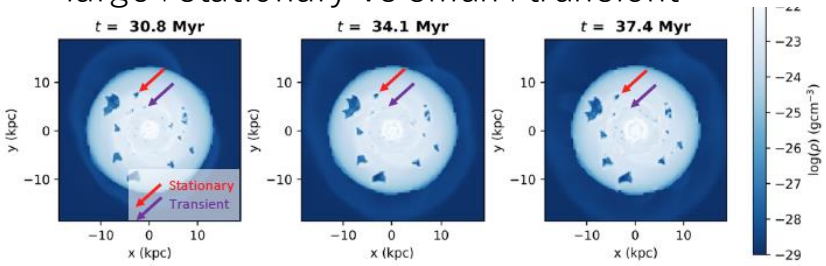

32: 2512.24299

From Nbody1 to Nbody7: the Growth of Sverre's Industry

Authors: Rainer Spurzem

Abstract: From NBODY1 to NBODY6 : The Growth of an Industry is the title of a 1999 invited review by Sverre Aarseth, for Publications of the Astronomical Society of the Pacific (PASP). I took this as an inspiration for the title of this paper; it describes how Sverres NBODY Industry has further grown since 90s of the previous century, and how it is further flourishing and hopefully developing, in his spirit, even after the sad news of his passing away reached us. My contact and friendship with Sverre started a few decades ago being sent to Cambridge to learn NBODY5, counting input parameters, and learning about the fact that even a sophisticated code (which had already at that time quite a history) requires permanent maintenance and bug fixes. Managed by Sverre, who relentlessly ran his code and responded to the widely spread crowd of customer colleagues. There has been a phase of massive and fast development and improvements due to vectorization, parallelization, GRAPE and GPU acceleration, and Sverre has been always on top of it if not ahead, but also fully adopting ideas of collaborators, once they tested well. NBODY6++GPU and NBODY7 entered the scene, and also recent new competitors, such as PETAR or BIFROST . We all have learnt a lot from Sverre, and strive to continue in his open-minded spirit, for open source and exchange. A striking evidence for the further growth of the industry is the number of papers here (and two of them follow in this session, but also in other sessions) using and further developing the aforementioned codes, as well as the occurrence of new and competing codes, which keep the field alive.

Table 1. Features of NBODY1-7, adopted with some updates from Spurzem and Kamlah (2023).

	ITS	ACS	KS	HITS	PN	AR	CC	MPI	GPU
NBODY1	✓								
NBODY2		✓		✓					
NBODY3	✓		✓						
NBODY4			✓	✓			✓		
NBODY5	✓	✓	✓		(✓)		✓		
NBODY6		✓	✓	✓			✓		
NBODY6GPU		✓	✓	✓	✓		✓		✓
NBODY6++		✓	✓	✓			✓	✓	
NBODY6++GPU		✓	✓	✓	(r)		✓	✓	✓
NBODY7		✓	✓	✓	✓	✓			✓

ITS	Individual time-steps (Aarseth 1985)
ACS	Ahmad–Cohen neighbour scheme (Ahmad and Cohen 1973)
KS	KS–regularization of few-body subsystems (Kustaanheimo and Stiefel 1965)
HITS	Hermite scheme and block steps (Makino and Aarseth 1992)
PN	Post-Newtonian (Kupi et al. 2006; Mikkola and Merritt 2008; Aarseth 2012)
AR	Algorithmic regularization (Mikkola and Merritt 2008)
CC	Classical chain regularization (Mikkola and Aarseth 1998)
MPI	Message Passing Interface, multi-node multi-CPU parallelization (Spurzem 1999)
GPU	use of GPU acceleration (Nitadori and Aarseth 2012; Berczik et al. 2013)

60: 2512.22429

Chain Reactions in Space: Analyzing the Impact of Satellite Collisions and Debris Accumulation

Authors: Mark Ballard, Guanqun Song, Ting Zhu

Abstract: The exponential increase in artificial satellites, growing from 852 in 2004 to over 9,000 in 2023, has intensified the risk of the Kessler Syndrome: a cascading chain reaction of orbital collisions. This paper analyzes the dynamics of space debris accumulation to identify the primary orbital features contributing to this systemic risk. We compiled and analyzed Two-Line Element (TLE) datasets from Space-Track.org and historical collision data using a Python-based data mining approach. Specifically, we derived satellite velocities using the Vis-Viva equation and evaluated the correlation of five key features, launch piece count, orbital period, apogee, perigee, and Radar Cross Section (RCS) size, with debris density. Our evaluation reveals that apogee and orbital period exhibit the strongest correlation with the risk of the Kessler Syndrome, indicating that satellites in higher orbits pose a disproportionately greater threat to long-term sustainability due to navigational constraints. Contrary to common assumptions, our data suggests that velocity and object size (RCS) show negligible direct correlation with collision incidence in the current dataset. Based on these findings, we propose mitigation strategies focusing on integrating AI-driven autonomous navigation systems and deploying advanced radiation-resistant shielding materials to enhance the resilience of high-orbit assets.

この文書は、人工衛星の急増が引き起こす宇宙のデブリ蓄積と衝突のリスク、特にケスラー効果について分析しています。

宇宙デブリとケスラー効果

•人工衛星の数は2004年の852から2023年には9,000を超え、急増している。
•ケスラー効果は、一定の衛星数を超えると衝突が連鎖的に発生し、デブリが増加する現象。
•2009年のアメリカのイリジウム衛星とロシアの軍事衛星の衝突は、2,300以上のデブリを生み出した。
•スペースXのスターリンクは、毎週1,600件の「近接遭遇」を記録しており、宇宙の混雑が深刻化している。

研究方法とデータ分析

•TLEデータセットを用いて、衛星の速度をビス-ビバ方程式で導出し、デブリ密度との相関を評価。
•主要な特徴として、打ち上げピース数、軌道周期、アポジー、ペリジー、レーダー反射断面積（RCS）を分析。
•アポジーと軌道周期がケスラー効果のリスクと強い相関を示し、高軌道の衛星が長期的な持続可能性に対して大きな脅威をもたらすことが判明。
•速度とRCSサイズは衝突発生率との直接的な相関がほとんどないことが示された。

提案される緩和策

•AI駆動の自律航行システムの統合と、放射線耐性シールド材料の展開を提案。
•高軌道の衛星のナビゲーション能力を向上させるため、より敏感なセンサーと高度なシステムが必要。
•衛星の設計を強化し、過酷な宇宙環境から保護するための新素材や自己修復技術の導入が推奨される。

結論

•衝突のリスクは年々増加しており、特に高軌道の衛星がケスラー効果のリスクを高める。
•衛星のナビゲーション能力を向上させることが、衝突のリスクを軽減する鍵となる。
•これらの提案は、宇宙資産の保護だけでなく、宇宙技術の安全性と信頼性を向上させることに寄与する。